# Proton superfluidity and charge radii in proton-rich calcium isotopes

A. J. Miller[1,2], K. Minamisono[1,2], A. Klose[3], D. Garand[1], C. Kujawa[3], J. D. Lantis[1,4], Y. Liu[5], B. Maaß[6], P. F. Mantica[7,4], W. Nazarewicz[7,2], W. Nörtershäuser[6], S. V. Pineda[3], P.-G. Reinhard[8], D. M. Rossi[6], F. Sommer[6], C. Sumithrarachchi[1], A. Teigelhöfer[9] and J. Watkins[1]

[1]National Superconducting Cyclotron Laboratory, Michigan State University, East Lansing, Michigan 48824, USA
[2]Department of Physics and Astronomy, Michigan State University, East Lansing, Michigan 48824, USA
[3]Department of Chemistry, Augustana University, Sioux Falls, South Dakota 57197, USA
[4]Department of Chemistry, Michigan State University, East Lansing, Michigan 48824, USA
[5]Physics Division, Oak Ridge National Laboratory, Oak Ridge, Tennessee 37831, USA
[6]Institut für Kernphysik, Technische Universität Darmstadt, 64289 Darmstadt, Germany
[7]Facility for Rare Isotope Beams, Michigan State University, East Lansing, Michigan 48824, USA
[8]Institut für Theoretische Physik, Universität Erlangen, D-91054 Erlangen, Germany
[9]TRIUMF, Vancouver, British Columbia V6T 2A3, Canada

**Arguably, one of the most important global properties of the atomic nucleus is its size. Experimentally determined nuclear charge radii carry unique information on the nuclear force and complex dynamics of protons and neutrons moving inside the nucleus. The intricate behavior of charge radii along the chain of Ca isotopes, including the unexpectedly large charge radius of neutron-rich $^{52}$Ca, pose a daunting challenge for nuclear theory[1]. Here we present the first measurements of the charge radii of proton-rich isotopes $^{36,37,38}$Ca, whose properties are impacted by the interplay between nuclear superfluidity and weak binding. The Nuclear Density Functional Theory shows that the novel Fayans pairing interaction[2] can successfully explain the behavior of charge radii from light to heavy Ca isotopes. Through this model, we show how the new data on $^{36,37,38}$Ca elucidate the nature of nuclear pairing in weakly bound proton-rich isotopes.**

At low excitation energies, atomic nuclei can be described as condensates of nucleonic (proton or neutron) pairs[3–5]. The resulting superfluid correlations profoundly influence the structure of nucleonic systems, such as finite nuclei and neutron stars[6]. In weakly-bound nuclei, pairing correlations can be enhanced due to the proximity of the particle continuum, which affects the asymptotic properties of density distributions. Moreover, due to the self-consistent feedback between particle and pairing fields, nuclear size is impacted by pairing correlations[7].

The interplay between nuclear size, pairing correlations, and weak binding takes a particularly dramatic form in spatially-extended, neutron-rich halo nuclei[8], such as $^{6}$He or $^{11}$Li. Indeed, their very existence comes from the additional pairing energy between valence neutrons. For weakly-bound, proton-rich nuclei, in which the Coulomb barrier has a localizing effect on the loosely bound or slightly unbound protons, pairing gives rise to the phenomenon of two-proton radioactivity[9]. The asymmetry in the energy spectra between mirror nuclei is another effect governed by a competition between weak binding and charge radius[10]. However, little is known about the radius of a weakly-bound proton-rich nucleus.

The charge radii of Ca isotopes are known up to $^{52}$Ca (ref.[1]). They exhibit a complicated behavior, with almost equal values in $^{40}$Ca and $^{48}$Ca, a local maximum at $^{44}$Ca, appreciable odd-even staggering, and a large value for $^{52}$Ca. Below the lightest stable $^{40}$Ca isotope, however, the charge radius is known only to $^{39}$Ca (ref.[11]), primarily due to the difficulty in the production of short-lived, proton-rich Ca nuclei. Theoretically, the pattern of charge radii along the Ca chain is difficult to explain[1,12–14].

Recent advances of radioactive beam production and manipulation techniques, that is to say, the fast in-flight production and separation[15] followed by gas stopping[16], made it possible to develop a good quality, high-rate beam of short-lived proton-rich Ca isotopes, including $^{36}$Ca with a half-life of $T_{1/2} = 102\,\mathrm{ms}$, which is sufficient for precise laser spectroscopy measurements. This production mechanism complements the capabilities of the isotope separator on line (ISOL) facilities (see Methods), where significant data on charge radii of selected elements have been obtained[17], including the charge radius of neutron-rich $^{52}$Ca with $T_{1/2} = 4.6\,\mathrm{s}$.

Our experiment was performed at the National Superconducting Cyclotron Laboratory at Michigan State University. A schematic of the complete setup is shown in Fig. 1. Projectile-fragmentation reactions of a 140 MeV/nucleon $^{40}$Ca primary beam on a thin transmission target (beryllium, 356 µm in thickness) were used to produce $^{36-39}$Ca isotopes (see Methods). The desired Ca ions were separated from the primary beam and other reaction products through the A1900 Fragment separator[15] based on magnetic rigidity selections. The selected fast Ca-ion beam was then injected into a gas cell stopper

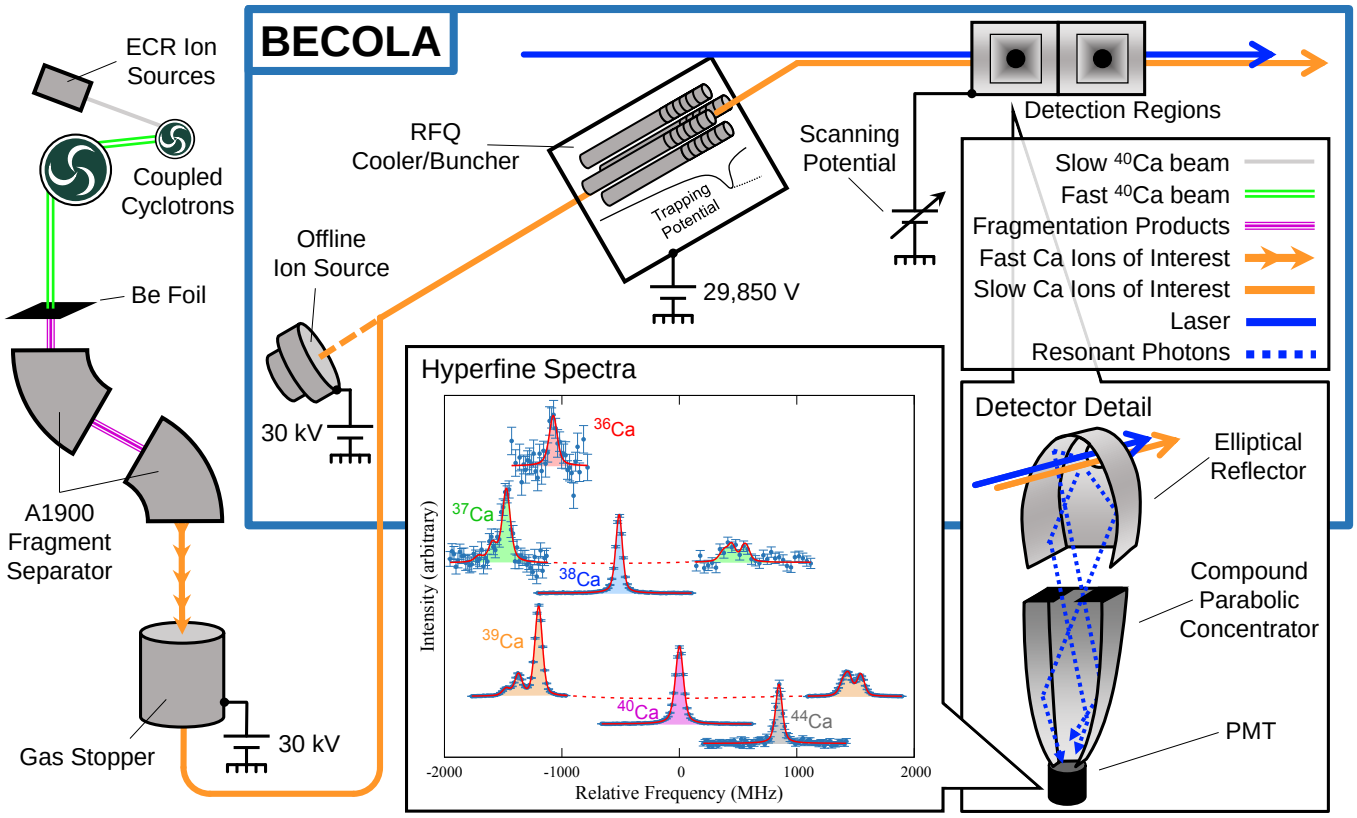


**Figure 1 | Experimental Setup and Hyperfine Spectra.** Projectile-fragment reaction was used to produce the fast Ca-ion beam, which was thermalized in the gas stopper, extracted at an energy of 30 keV, and transported to the BECOLA facility. Laser resonant fluorescence was detected using bunched-beam collinear laser spectroscopy. An offline ion source at BECOLA was used to produce stable Ca as needed for the reference measurements taken every several hours. The hyperfine spectra of the $4s\ ^2S_{1/2} \leftrightarrow 4p\ ^2P_{3/2}$ transition in $^{36-40,44}$Ca are shown as a function of the frequency relative to the centroid of $^{40}$Ca. The peaks were fit using a pseudo-Voigt profile (solid red lines), and isotope shifts were deduced from the difference of each isotope's centroid from that of $^{40}$Ca.

filled with a helium buffer gas[16], and the ions were thermalized. Singly-charged Ca ions of one desired mass were extracted at an energy of 30 keV after the stopping range selection in the cell, and the low-energy beam was transported to the BECOLA facility[18,19].

At BECOLA, the ion beam was first introduced into a helium buffer gas filled radio-frequency quadrupole cooler/buncher[20]. Ions were trapped in the cooler/buncher, further cooled (improving beam emittance) and periodically extracted at an approximate energy of 29 850 eV as ion beam bunches. The time spread of an ion bunch was set to ∼1 µs (full width at the half-maximum) by adjusting the radio-frequency and release potential. The narrow time spread is critical for a high sensitivity measurement as it reduces background significantly[21,22]. The bunched ion beam was then overlapped with laser light and co-propagated for bunched-beam collinear laser spectroscopy.

Laser-induced fluorescence was detected using two sets of photon detection systems (see Methods). The $4s\ ^2S_{1/2} \leftrightarrow 4p\ ^2P_{3/2}$ transition in CaII at 393 nm was probed to measure the hyperfine spectrum. The timing between the ion bunches was optimized based on the lifetime of Ca isotopes to maximize the signal to noise ratio (see Methods). A sawtooth-pattern ramping voltage with discrete steps was applied to the photon detection system to vary the incoming ion beam velocity. Ions experienced a Doppler-shifted laser frequency and the hyperfine spectrum was scanned at a fixed laser frequency. Spectra of stable $^{40,44}$Ca, which were produced in an offline ion source, were measured periodically to be used as a reference of the isotope shift, and also for ion beam energy calibration purposes (see Methods). The obtained spectra of Ca isotopes are included in Fig. 1.

The $^{37,39}$Ca isotopes, which have nuclear ground-state spin of $I = 3/2$, show hyperfine splittings with six allowed transitions, whereas single peaks were observed for the even Ca isotopes as they have $I = 0$. The hyperfine

**Table 1 | Isotope shifts and deduced differential mean-square charge radii.** The numbers in the parentheses and brackets are the statistical and systematic uncertainties, respectively. The differential m.s. charge radius of $^{39}$Ca is consistent with the previous value[11] of $-0.127(20)\,\mathrm{fm}^2$. The half-life ($T_{1/2}$), bunching period ($T_b$), and rates at the cooler/buncher for each isotope are also included.

| $A$ | $\delta\nu^{40,A}$ (MHz) | $\delta\langle r^2\rangle$ (fm$^2$) | $T_{1/2}$ (ms) | $T_b$ (ms) | Rate (1/s) |
|---|---|---|---|---|---|
| 36 | −1073.8(60)[43] | −0.196(21)[16] | 102 | 180 | 50 |
| 37 | −766.1(47)[49] | −0.205(15)[17] | 181 | 330 | 960 |
| 38 | −513.1(3)[17] | −0.0797(11)[63] | 440 | 220 | 13500 |
| 39 | −230.5(2)[18] | −0.1060(7)[64] | 859.6 | 30 | 60000 |

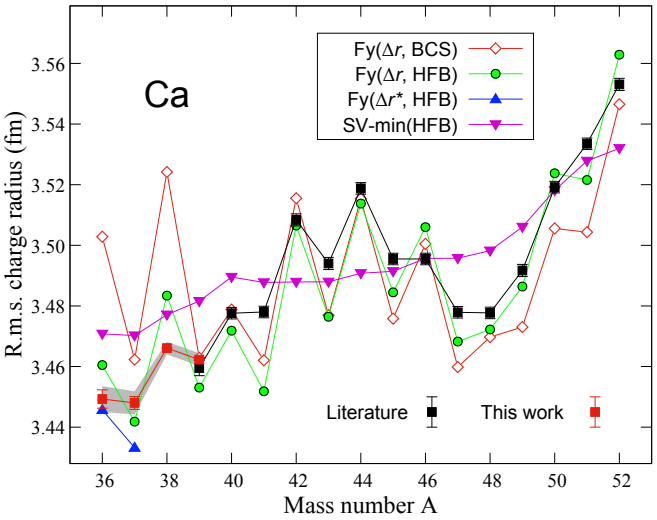


**Figure 2 | Charge radii of Ca isotopes.** The charge radii measured in this work (red squares) and previous experimental values (black squares) are compared to DFT predictions of SV-min (HFB), Fy($\Delta r$,BCS), Fy($\Delta r$,HFB), and Fy($\Delta r^*$,HFB) models. The values of Fy($\Delta r^*$,HFB) for $A > 37$ are very close to Fy($\Delta r$,HFB) results; hence, they are not shown. The r.m.s. charge radii were obtained using the known charge radius of $^{40}$Ca (ref.[23]), and its error has been incorporated into the systematic uncertainty (the gray band).

spectra were fit using a pseudo-Voigt profile to reproduce line-shape broadening due mostly to the fluctuation of the applied potential (see Methods). The resulting centroids of the hyperfine spectra of $^{36-39}$Ca were compared to the reference measurement of $^{40}$Ca, and isotope shifts $\delta\nu^{40,A}$ were extracted, which are summarized in Table 1.

The differential mean-square (m.s.) charge radius $\delta\langle r^2\rangle^{A,A'} = \langle r^2\rangle^{A'} - \langle r^2\rangle^{A}$ can be obtained from the isotope shift between isotopes $A$ and $A'$ through

$$\delta\nu^{A,A'} = \nu^{A'} - \nu^{A} = k\frac{m_{A'} - m_A}{m_{A'}m_A} + F\delta\langle r^2\rangle^{A,A'} \quad (1)$$

where $k$ and $F$ are the mass and field shift coefficient, respectively, and determined by the orbital electronic configuration, and $m$ is the atomic mass. The atomic factors of the $^2S_{1/2}\leftrightarrow{}^2P_{3/2}$ transition in CaII used in the present study were determined as $k = 409.35(42)$ GHz/amu and $F = -284.7(82)\,\mathrm{MHz/fm}^2$ from a King plot analysis[24]. The obtained differential m.s. charge radii are summarized in Table 1 and the root-mean-square (r.m.s.) charge radii are shown in Fig. 2. The present data are shown in solid red squares and other known values are also plotted in solid black squares. The obtained $\delta\langle r^2\rangle$ of $^{39}$Ca is consistent with the known value[11], and our experiment has reduced the uncertainty by a factor of 3.

Overall, the charge radii decrease towards neutron deficient isotopes across the neutron $N = 20$ shell closure, which makes sharp contrast with the discontinuity seen at the $N = 28$ shell closure. Similar behavior has been observed in the neighboring Ar (ref.[25]) and K (ref.[26]) isotopic chains. The new charge radii also show an odd-even staggering, though the amplitude of the effect is smaller than around $N = 24$.

Charge radii of proton-rich Ca isotopes are strongly impacted by nuclear superfluidity. Indeed, as seen in Fig. 3(a), for $^{36-38}$Ca the $0d_{3/2}$ valence proton shell is weakly bound and the next $0f_{7/2}$ orbital lies above the Coulomb barrier. This means that pairing correlations due to the scattering of proton pairs from the bound proton states into the proton continuum are expected to leave an imprint on the properties of these nuclei. In the presence of low-lying continuum space, the standard Hartree-Fock (HF)+ Bardeen-Cooper-Schrieffer (BCS) treatment of nucleonic pairing becomes questionable as the resulting particle and pair densities are not spatially localized and acquire an unphysical gas component because of the nonzero occupation probabilities of unbound states. To analyze these effects in more detail, we use nuclear Density Functional Theory (DFT) with realistic energy density functionals. As a typical representative of standard functionals, we use the parametrization SV-min[27]. These models employ a highly elaborate functional for the mean field together with a contact force for pairing augmented by some density dependence[28]. The performance of these models on global trends of nuclear gross properties is superb, but their simple pairing functional fails to describe isotope shifts and odd-even staggering of charge radii in medium-light nuclei[14]. To overcome this hurdle, a nuclear density functional with a more elaborate pairing functional was employed by Fayans *et al.*[29]. Its essential new piece was a coupling of pairing density to the gradient of normal density. In ref.[14], this functional was refitted exactly to the same pool of fit data as SV-min and additional specific information on isotopic shifts of radii in neutron-rich Ca

leading to a functional called Fy($\Delta r$). This fit used the HF+BCS approximation to pairing. Hence we shall refer to this model as Fy($\Delta r$,BCS).

As said above, the BCS approximation becomes unsafe for weakly bound nuclei. To get some insight on the magnitude of the continuum gas effect, Fig. 3(c) shows the occupations of single-proton states in $^{36}$Ca obtained in Fy($\Delta r$,BCS) model (diamonds), and Fig. 3(b) displays the corresponding single-proton r.m.s. radii. The ground-state of $^{36}$Ca is predicted to have a nonzero proton pairing gap, which results in nonzero occupations of unbound single-proton orbits above the $Z = 20$ gap. Since these states are formally not localized, their r.m.s. radii become unphysically large.

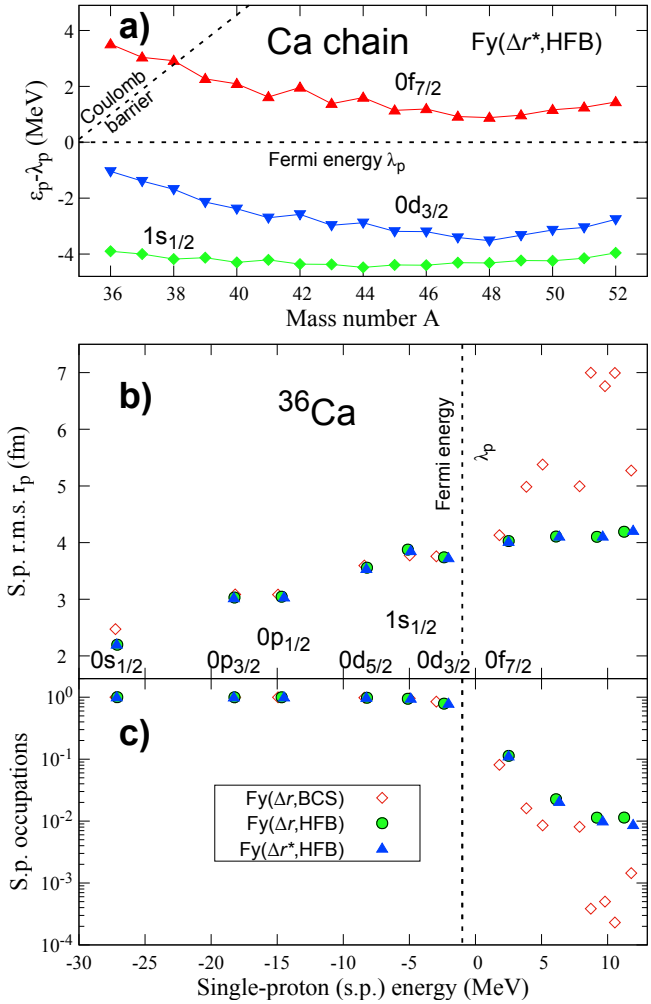


**Figure 3 | Single-proton structure.** (a) Canonical single-proton energies ($\varepsilon_p$) (expectation values of the self-consistent mean-field Hamiltonian in the canonical states[30]) relative to the proton Fermi level ($\lambda_p$) for the Ca chain obtained in Fy($\Delta r^*$,HFB). The position of the Coulomb barrier is indicated. For the proton-rich isotopes of $^{36-38}$Ca, the unbound shell $0f_{7/2}$ is predicted to lie above the Coulomb barrier, i.e., it is expected to be affected by proton continuum effects. (b) r.m.s. radii and (c) occupations of canonical single-proton states in $^{36}$Ca obtained in Fy($\Delta r$,BCS), Fy($\Delta r$,HFB), and Fy($\Delta r^*$,HFB) models.

To overcome this problem, one has to resort to the full Hartree-Fock-Bogolyubov (HFB) formalism, which - for particle-bound nuclei - guarantees the spatial localization of nuclear densities and fields[30,31]; hence, preventing the particle gas from appearing. To this end, we re-optimized the original Fy($\Delta r$,BCS) model within the full HFB framework. The resulting energy density functionals are Fy($\Delta r$,HFB) and Fy($\Delta r^*$,HFB) (see Methods). To probe the impact of the charge radius of $^{36}$Ca obtained in this Letter on model predictions, in the dataset of Fy($\Delta r^*$,HFB) we also included the constraint on $\delta\langle r^2\rangle$[40,36].

The localized single-particle orbits of HFB are called canonical (or natural) states[30]; those are the eigenvalues of the single-particle density matrix. The single-particle r.m.s. proton radii of canonical states in $^{36}$Ca obtained in Fy($\Delta r$,HFB) and Fy($\Delta r^*$,HFB) models are displayed in Fig. 3(b). The r.m.s. radii of unbound HFB orbits behave very regularly and do not show the marked increase which is seen for BCS orbits. This allows the HFB occupations of unbound proton states to stay somehow larger than the BCS occupations, see Fig. 3(c), without diluting the whole nucleus. It is interesting to note that BCS at least tries to reduce the problem of continuum gas by significant reduction of continuum occupations.

Charge radii of Ca isotopes predicted by SV-min (HFB), Fy($\Delta r$,BCS), Fy($\Delta r$,HFB), and Fy($\Delta r^*$,HFB) models are shown in Fig. 2. The SV-min (HFB) results exhibit characteristic monotonic dependence on $A$ and practically nonexistent odd-even effect[1,13,14]. Due to the presence of proton gas, the functional Fy($\Delta r$,BCS) dramatically overestimates charge radii in the proton-rich isotopes of $^{36,38}$Ca. On the other hand, the Fy($\Delta r$,HFB) and Fy($\Delta r^*$,HFB) models provide a remarkably good overall description of experimental data. It is noted that values of Fy($\Delta r^*$,HFB) above $A = 37$ are not shown in Fig. 2 due to their similarity to Fy($\Delta r$,HFB). Both models tend to slightly overestimate the odd-even staggering of charge radii, but this is a minor deficiency considering the scale of this effect. The unexpectedly large charge radius of $^{52}$Ca (ref.[1]) is well explained by the Fy($\Delta r$,HFB) and Fy($\Delta r^*$,HFB) models, and their description of $A > 48$ radii has even been improved.

The comparison between SV-min (HFB) and Fy($\Delta r$,HFB)/Fy($\Delta r^*$,HFB) results shows the importance of the non-standard density dependence of Fayans functional, especially its novel pairing term. The ability to accommodate the radii along the Ca chain can be clearly associated with two particular

features of the Fayans functional, mainly the gradient coupling in the pairing functional and a gradient term in the surface energy[14]. The pairing gradient term was necessary to reproduce the demanding $\delta\langle r^2\rangle^{48,44}$ and $\delta\langle r^2\rangle^{48,52}$ values. The Fayans pairing functional turned out to be flexible enough to account also for $\delta\langle r^2\rangle^{40,36}$ delivering in Fy($\Delta r^*$,HFB) a very good agreement with experimental charge radius of $^{36}$Ca, while maintaining the same descriptive power as Fy($\Delta r$,HFB) for $A > 37$.

The new charge radii data on proton-rich Ca isotopes demonstrated the need for the careful treatment of proton superfluid correlations in the presence of low-lying continuum states. It is remarkable, that the new Fy($\Delta r$,HFB) and Fy($\Delta r^*$,HFB) models, based on HFB formalism and the Fayans energy density functional, developed with the focus on $^{36-38}$Ca, also improve description of neutron-rich isotopes all the way to, and including, $^{52}$Ca.

---


[1] Ruiz, R. F. G. *et al.* Unexpectedly large charge radii of neutron-rich calcium isotopes. *Nat. Phys.* **12**, 594 (2016). URL `http://dx.doi.org/10.1038/nphys3645`.

[2] Fayans, S. A. Towards a universal nuclear density functional. *JETP Lett.* **68**, 169 (1998). URL `http://dx.doi.org/10.1134/1.567841`.

[3] Bohr, A., Mottelson, B. R. & Pines, D. Possible analogy between the excitation spectra of nuclei and those of the superconducting metallic state. *Phys. Rev.* **110**, 936–938 (1958). URL `https://link.aps.org/doi/10.1103/PhysRev.110.936`.

[4] Brink, D. M. & Broglia, R. A. *Nuclear Superfluidity, Pairing in Finite Systems* (Cambridge University Press, Cambridge, UK, 2005). URL `http://admin.cambridge.org/academic/subjects/physics/particle-physics-and-nuclear-physics/nuclear-superfluidity-pairing-finite-systems`.

[5] Broglia, R. A. & Zelevinski, V. (eds.) *50 Years of Nuclear BCS* (World Scientific, 2012).

[6] Dean, D. J. & Hjorth-Jensen, M. Pairing in nuclear systems: from neutron stars to finite nuclei. *Rev. Mod. Phys.* **75**, 607–656 (2003). URL `https://link.aps.org/doi/10.1103/RevModPhys.75.607`.

[7] Dobaczewski, J., Nazarewicz, W. & Reinhard, P.-G. Pairing interaction and self-consistent densities in neutron-rich nuclei. *Nucl. Phys. A* **693**, 361 – 373 (2001). URL `http://www.sciencedirect.com/science/article/pii/S0375947401009939`.

[8] Jensen, A. S., Riisager, K., Fedorov, D. V. & Garrido, E. Structure and reactions of quantum halos. *Rev. Mod. Phys.* **76**, 215–261 (2004). URL `https://link.aps.org/doi/10.1103/RevModPhys.76.215`.

[9] Pfützner, M., Karny, M., Grigorenko, L. V. & Riisager, K. Radioactive decays at limits of nuclear stability. *Rev. Mod. Phys.* **84**, 567–619 (2012). URL `https://link.aps.org/doi/10.1103/RevModPhys.84.567`.

[10] Agrawal, B. K., Sil, T., Samaddar, S. K., De, J. N. & Shlomo, S. Coulomb energy differences in mirror nuclei revisited. *Phys. Rev. C* **64**, 024305 (2001). URL `https://link.aps.org/doi/10.1103/PhysRevC.64.024305`.

[11] Vermeeren, L. *et al.* The mean square nuclear charge radius of $^{39}$Ca. *J. Phys. G* **22**, 1517 (1996).

[12] Caurier, E., Langanke, K., Martínez-Pinedo, G., Nowacki, F. & Vogel, P. Shell model description of isotope shifts in calcium. *Phys. Lett. B* **522**, 240–244 (2001).

[13] Minamisono, K. *et al.* Charge radii of neutron deficient $^{52,53}$Fe produced by projectile fragmentation. *Phys. Rev. Lett.* **117**, 252501 (2016).

[14] Reinhard, P.-G. & Nazarewicz, W. Toward a global description of nuclear charge radii: Exploring the fayans energy density functional. *Phys. Rev. C* **95**, 064328 (2017). URL `https://link.aps.org/doi/10.1103/PhysRevC.95.064328`.

[15] Morrissey, D. J., Sherrill, B. M., Steiner, M., Stolz, A. & Wiedenhoever, I. Commissioning the A1900 projectile fragment separator. *Nucl. Instrum. Methods Phys. Res. B* **204**, 90–96 (2003).

[16] Cooper, K. *et al.* Extraction of thermalized projectile fragments from a large volume gas cell. *Nucl. Instrum. Methods Phys. Res. A* **763**, 543–546 (2014).

[17] Campbell, P., Moore, I. D. & Pearson, M. R. Laser spectroscopy for nuclear structure physics. *Prog. Part. Nucl. Phys.* **86**, 127 (2016).

[18] Minamisono, K. *et al.* Commissioning of the collinear laser spectroscopy system in the BECOLA facility at NSCL. *Nucl. Instrum. Methods Phys. Res. A* **709**, 85–94 (2013).

[19] Rossi, D. M. *et al.* A field programmable gate array-based time-resolved scaler for collinear laser spectroscopy with bunched radioactive potassium beams. *Rev. of Sci. Instrum.* **85**, 093503 (2014).

[20] Barquest, B. R. *et al.* RFQ beam cooler and buncher for collinear laser spectroscopy of rare isotopes. *Nucl. Instrum. Method Phys. Res. A* **866**, 18 (2017).

[21] Nieminen, A. *et al.* On-line ion cooling and bunching for collinear laser spectroscopy. *Phys. Rev. Lett.* **88**, 094801 (2002).

[22] Campbell, P. *et al.* Laser spectroscopy of cooled zirconium fission fragments. *Phys. Rev. Lett.* **89**, 082501 (2002).

[23] Angeli, I. & Marinova, K. P. Table of experimental nuclear ground state charge radii: An update. *Atomic Data and Nuclear Data Tables* **99**, 69–95 (2013).

[24] Shi, C. *et al.* Unexpectedly large difference of the electron density at the nucleus in the $4p\,^2P_{1/2,3/2}$ fine-structure doublet of ca$^+$. *Applied Physics B* **123**, 2 (2016). URL `https://doi.org/10.1007/s00340-016-6572-z`.

[25] Klein, A. *et al.* Moments and mean square charge radii of short-lived argon isotopes. *Nucl. Phys. A* **607**, 1–22 (1996).

[26] Rossi, D. M. *et al.* Charge radii of neutron-deficient $^{36}$K and $^{37}$K. *Phys. Rev. C* **92**, 014305 (2015). URL `http://link.aps.org/doi/10.1103/PhysRevC.92.014305`.

[27] Klüpfel, P., Reinhard, P.-G., Bürvenich, T. J. & Maruhn, J. A. Variations on a theme by Skyrme: A systematic study of adjustments of model parameters. *Phys. Rev. C* **79**, 034310 (2009).

[28] Bender, M., Heenen, P.-H. & Reinhard, P.-G. Self-

consistent mean-field models for nuclear structure. *Rev. Mod. Phys.* **75**, 121–180 (2003).

[29] Fayans, S. A., Tolokonnikov, S. V., Trykov, E. L. & Zawischa, D. Nuclear isotope shifts within the local energy-density functional approach. *Nucl. Phys. A* **676**, 49 (2000).

[30] Dobaczewski, J. *et al.* Mean-field description of ground-state properties of drip-line nuclei: Pairing and continuum effects. *Phys. Rev. C* **53**, 2809–2840 (1996). URL `https://link.aps.org/doi/10.1103/PhysRevC.53.2809`.

[31] Dobaczewski, J., Flocard, H. & Treiner, J. Hartree-Fock-Bogolyubov description of nuclei near the neutron-drip line. *Nucl. Phys. A* **422**, 103 – 139 (1984). URL `http://www.sciencedirect.com/science/article/pii/0375947484904330`.

# METHODS

## Isotope production technique

In the present study, a projectile-fragmentation reaction was used to produce the isotopes in-flight. This reaction is characterized by the reaction products being emitted in a narrow forward solid angle at nearly the primary-beam velocity. This makes the fast and efficient selection of fragments possible without regards to their chemical properties by using a magnetic spectrometer.

In the ISOL technique utilized at other facilities, rare isotopes are extracted from thick targets bombarded by light ions. High quality, high intensity beams are available at low energy (∼60 keV) for certain elements. The ISOL production method, however, suffers from a serious limitation due to long release times from thick targets. This can lead to large decay losses for nuclides that have long diffusion and/or effusion times and with short half-lives at the limits of the nuclear chart.

**The photon detection system** Two sets of photon detection systems were used to detect the resonant fluorescence; each detector comprised a light collection section and a photomultiplier tube. The collection sections contained an ellipsoidal reflector, which focuses the signal tighter than background light, and a following compound parabolic concentrator, which further eliminates background based on its wider incident angles.

**The laser system** A Sirah Matisse TS Ti:Sapphire ring laser was used to produce 787 nm light, and a SpectraPhysics WaveTrain generated the 393 nm light by frequency doubling the 787 nm light. The Ti:Sapphire laser frequency was locked using a HighFinesse WSU-30 wavelength meter calibrated by a frequency stabilized He-Ne laser. Laser power at the interaction region was stabilized at 300 µW using a laser power controller[32].

**Optimization of bunching period** The bunching period was chosen to maximize the signal-to-noise ratio for each isotope. An increased bunching period $T_b$ reduces the background as $B(T_b) \propto 1/T_b$ for a given time spread of an ion bunch. The signal is proportional to the number of trapped ions, which depends on the ion rate and the decay loss, as $S(T_b) \propto (1/\lambda)(1-e^{-\lambda T_b})/T_b$, where $\lambda$ is the decay constant. Signal-to-noise ratio (SNR) can then be evaluated as

$$\mathrm{SNR} = \frac{S(T_b)}{\sqrt{B(T_b)}} \propto \frac{(1/\lambda)(1-e^{-\lambda T_b})}{\sqrt{T_b}}. \tag{2}$$

The SNR is maximized at $T_b \approx 1.3/\lambda \approx 1.8 \times T_{1/2}$. This condition does not depend on the ion rate, as long as the space charge of the trapped ions does not disturb the emittance of the released ion bunches. The bunching periods of $^{36,37}$Ca were chosen based directly on the lifetime, however due to the increased rates, the bunching periods of $^{38,39}$Ca were shortened to avoid space charge effects. The bunching periods and approximate rates for each isotope are summarized in Table 1.

**Energy calibration with stable $^{40,44}$Ca** The ion's rest-frame resonant laser frequency can be obtained from the set laser frequency and the total potential applied to the ion beam, which is the sum of potentials applied to the cooler/buncher and the photon detection system. The total potential makes the largest contribution to the uncertainty in the determination of the charge radius since the potential at which ions are released from the cooler/buncher is not directly known and the uncertainty is estimated to be 10 V. In order to eliminate this uncertainty, a well known isotope shift between stable $^{40}$Ca and $^{44}$Ca isotopes ($\delta\nu^{40,44} = 850.231(65)$ MHz[24]) was used to calibrate the total potential. This calibration is the predominant source of systematic uncertainty. The spectroscopy of $^{40,44}$Ca was performed using ions produced by an offline discharge plasma ion source[33] and introduced into the cooler/buncher. The calibration was performed every several hours throughout the experiment to monitor and correct for the time dependent variation of the total potential, and was also affected by fluctuations of the laser frequency. By examining the variations of the calibration throughout the experiment, the systematic uncertainty due to both the laser frequency and total potential was determined.

**Hyperfine spectra fitting procedure** All peaks were fit using an asymmetric pseudo-Voigt function[34]. For $^{36,37}$Ca, the lineshape (asymmetry, which was negligibly small, and Lorentz fraction) of the peaks was constrained to match those obtained from the $^{40}$Ca reference, however the line-width was allowed to vary due to the longer running time. The $^{40,44}$Ca peaks were typically ∼75 MHz wide, while $^{37,38}$Ca which required the longest running times, had line-widths of ∼80 MHz. In $^{39}$Ca ($I = 3/2$), all six peaks of the hyperfine spectra were fit with a common lineshape and width, and their positions were obtained by fitting the 3 hyperfine coupling constants ($A^{\mathrm{HF}}_{\mathrm{lower}}, A^{\mathrm{HF}}_{\mathrm{upper}}, B^{\mathrm{HF}}_{\mathrm{upper}}$), with the upper and lower levels shifted by,

$$\Delta E = \frac{K}{2}A^{\mathrm{HF}} + \frac{3K(K+1) - 4I(I+1)J(J+1)}{8I(2I-1)J(2J-1)}B^{\mathrm{HF}} \tag{3}$$

where $K = F(F+1) - I(I+1) - J(J+1)$, $F$ is the quantum number defined by the vector $\mathbf{F} = \mathbf{I} + \mathbf{J}$, and $I$ and $J$ are the nuclear and atomic spins respectively. The height of each peak was allowed to vary freely in $^{39}$Ca, and because of the excellent statistics, the relative intensity of each peak was used as a constraint in the fit of the $^{37}$Ca spectrum (also $I = 3/2$).

**Density functional theory calculations** Our DFT calculations were carried out with the original SV-min (ref.[27]) and Fy($\Delta r$,BCS) (ref.[14]) energy density functionals, as well as new functionals Fy($\Delta r$,HFB) and Fy($\Delta r^*$,HFB) developed in this work. In general, our EDF optimization methodology closely followed that of ref.[14]. Namely, by carefully selecting datasets of experimental data used in optimization, we generate func-

tionals to study questions pertaining to different observables. The functional SV-min was optimized to the basic dataset of ref.[27] containing 224 experimental data points, including binding energies, diffraction radii, surface thickness, charge radii, and spin-orbit splitting. The functional Fy($\Delta r$,BCS) was constrained by the basic dataset of SV-min as well as by additional data on differential charge radii of Ca isotopes ($\delta\langle r^2\rangle^{48,40}$, $\delta\langle r^2\rangle^{48,44}$, $\delta\langle r^2\rangle^{52,48}$). Pairing information is included here in terms of neutron and proton odd-even binding energy staggering $\Delta_E^{(3)}$ extracted from three-point binding-energy differences.

Unlike in Fy($\Delta r$,BCS), which was developed under the HF+BCS protocol, pairing correlations in Fy($\Delta r$,HFB) and Fy($\Delta r^*$,HFB) are treated within the full HFB framework using the techniques of[36] and without employing the gap stabilization method[37]. Moreover, to constrain the pairing term, three-point binding energy differences $\Delta_E^{\rm ee}$ involving ground states of even-even nuclei[14] were employed rather than $\Delta_E^{(3)}$. As discussed in ref.[38], for open-shell systems, $\Delta_E^{\rm ee}$ is simply related to the pairing rotational moment of inertia and is superior to $\Delta_E^{(3)}$, which involve properties of odd-mass systems that depend on poorly known time-odd fields impacting individual orbits occupied by an odd nucleon. We have checked within the BCS method that the fit to even-even gaps produces practically the same pairing gaps as the fit to $\Delta_E^{(3)}$ used in Fy($\Delta r$,BCS). Moreover, the dataset of Fy($\Delta r^*$,HFB) also includes the value of $\delta\langle r^2\rangle^{40,36}$. For the purpose of this work, the functional SV-min has also been re-optimized in the HFB variant; the resulting model is called SV-min (HFB), again, using here $\Delta_E^{\rm ee}$ as pairing information.

To compute odd-$A$ nuclei, we applied the standard uniform filling approximation to blocking[39,40], in which an unpaired nucleon is put with equal probability in each of the degenerate magnetic sub-states. To find the ground state, blocked calculations were carried out for all orbitals near the Fermi energy and the blocked state with lowest energy were selected.

It is to be noted that the excellent description of charge radii in the Ca chain with $39 \leq A \leq 50$ was obtained in previous calculations with FaNDF$^0$, DF3, and DF3-a Fayans functionals[29 41,42]. The functionals Fy($\Delta r$,BCS), Fy($\Delta r$,HFB) and Fy($\Delta r^*$,HFB) used here derive from FaNDF$^0$.

Finally, it has recently been suggested that the differences in the charge radii of mirror nuclei can be used for constraining the neutron equation of state for use in astrophysics[43]. Our theoretical results for $^{36-38}$Ca show that without an advanced approach to proton pairing in weakly bound proton-rich mirror partners, it will be difficult to arrive at precise predictions.

**Acknowledgments** This work was supported in part by the National Science Foundation, Grants No. PHY-15-65546; the U.S. Department of Energy, National Nuclear Security Administration, grant No. DE-NA0002924; the U.S. Department of Energy, Office of Science, Office of Nuclear Physics, Grant Nos. DE-SC0013365, DE-SC0018083, DE-AC02-06CH11357, and DE-AC05-00OR22725 with UT-Battelle, LLC; the German Research Foundation Contract No. SFB 1245; the German Federal Ministry of Education and Research (BMBF), Grants No. 05P12RFFTG and No. 015P15SJCIA.

**Author contributions** A.J.M., K.M., A.K., D.G., J.D.L., Y.L., P.F.M., S.V.P., D.M.R., F.S., C.S., and A.T. performed the experiment. A.J.M., C.K., B.M., W.Nörtershäuser, and J.W. designed and installed the upgraded photon detection system. A.J.M. performed data analysis and discussed with K.M., A.K., W.Nörtershäuser, and D.M.R.. W.Nazarewicz and P.G.R. performed theoretical analysis. A.J.M., K.M., W.Nazarewicz, and P.G.R. prepared the figures. A.J.M., K.M., W.Nazarewicz, and P.G.R. prepared the manuscript. All authors discussed the results and contributed to the manuscript at all stages.

**Author information** The authors declare no competing financial interests. Readers are welcome to comment on the online version of the paper. Correspondence and requests for materials should be addressed to K.M. (minamiso@nscl.msu.edu).

[32] See `http://www.brocktoneo.com` for information on the laser-power controller. (accessed in 2016.).

[33] Ryder, C. A. *et al.* Population distribution subsequent to charge exchange of 29.85 kev ni$^+$ on sodium vapor. *Spectrochimica Acta Part B* **113**, 16–21 (2015).

[34] Stancik, A. L. & Brauns, E. B. A simple asymmetric lineshape for fitting infrared absorption spectra. *Vibrational Spectroscopy* **47**, 66–69 (2008).

[35] Klüpfel, P., Reinhard, P.-G., Bürvenich, T. J. & Maruhn, J. A. Variations on a theme by Skyrme: A systematic study of adjustments of model parameters. *Phys. Rev. C* **79**, 034310 (2009).

[36] Reinhard, P.-G., Bender, M., Rutz, K. & Maruhn, J. An HFB scheme in natural orbitals. *Z. Phys. A* **358**, 277 (1997). Http://www.arxiv.org/abs/nucl-th/9705054.

[37] Erler, J., Klüpfel, P. & Reinhard, P.-G. A stabilized pairing functional. *Eur. Phys. J. A* **37**, 81 (2008).

[38] Hinohara, N. & Nazarewicz, W. Pairing Nambu-Goldstone modes within nuclear Density Functional Theory. *Phys. Rev. Lett.* **116**, 152502 (2016).

[39] Duguet, T., Bonche, P., Heenen, P.-H. & Meyer, J. Pairing correlations. i. description of odd nuclei in mean-field theories. *Phys. Rev. C* **65**, 014310 (2001).

[40] Schunck, N. *et al.* One-quasiparticle states in the nu-

clear energy density functional theory. *Phys. Rev. C* **81**, 024316 (2010). URL https://link.aps.org/doi/10.1103/PhysRevC.81.024316.

[41] Tolokonnikov, S. V. & Saperstein, E. E. Description of superheavy nuclei on the basis of a modified version of the df3 energy functional. *Phys. At. Nucl.* **73**, 1684 (2010).

[42] Saperstein, E. E. & Tolokonnikov, S. V. Self-consistent theory of finite Fermi systems and radii of nuclei. *Phys. At. Nucl.* **74**, 1277 (2011). URL https://doi.org/10.1134/S1063778811090109.

[43] Brown, B. A. Mirror charge radii and the neutron equation of state. *Phys. Rev. Lett.* **119**, 122502 (2017). URL https://link.aps.org/doi/10.1103/PhysRevLett.119.122502.